Available online at www.sciencedirect.com
SCIENCE DIRECT®
Composites Science and Technology 65 (2005) 621–634
COMPOSITES SCIENCE AND TECHNOLOGY
www.elsevier.com/locate/compscitech

Viscoelastic response of woven composite substrates

P. Shrotriya *, N.R. Sottos

Department of Theoretical and Applied Mechanics, University of Illinois at Urbana-Champaign, Urbana, IL, USA

Received 1 February 2004; received in revised form 27 August 2004; accepted 9 September 2004
Available online 22 October 2004

Abstract

Micromechanical models are developed to predict the time and temperature dependent response of woven composite substrates used in multilayer printed circuit boards. In the first part of this study, the elastic–viscoelastic correspondence principle is applied to previously reported elastic micromechanical models. The time-dependent creep compliance of a particular composite substrate (7628 style fabric) is predicted and compared with experimental measurements. Several deficiencies and possible modifications to the analytical models are identified. In the second part, a finite element model is adopted to examine the influence of boundary conditions and relevant matrix properties on the composite viscoelastic response. Parametric studies reveal the importance of shifts in the relaxation spectrum local to the matrix in the high volume fraction fiber bundles and the need to account for time-dependent Poisson's ratio of the matrix.

1. Introduction

Multilayer printed circuit boards (PCBs) are used extensively in electronic packaging assemblies. The boards consist of multiple layers of woven glass/epoxy composite substrate sandwiched between copper foils. A large number of plain weave fabric styles are currently used in circuit board design. The fabric styles are often unbalanced, i.e. the warp and fill directions include different numbers of fiber bundles or different size fiber diameters. Because of the variation in fiber bundle sizes, geometry of the undulating fiber bundles is different and depends on the fabric styles. Hence, composite substrates with different fabric styles have very different properties. Furthermore, the same fabric style has different properties in the warp and fill directions. Sottos et al. [1] measured significant differences in the fabric geometry (bundle size, crimp, etc.), the elastic moduli, and coefficients of thermal expansion (CTE) in the warp and fill directions of two common substrates for multilayer circuit boards. Wu et al. [2] and Yuan and Falanga [3] characterized the CTE of substrates below the matrix glass transition temperature and detected higher CTE values in the fill direction.

During relamination, the boards are heated above the matrix glass transition temperature (T_g) for an extended period of time. At temperatures near the glass transition, viscoelastic processes dominate the matrix response. The resulting time–temperature dependence of composite substrate properties leads to undesirable dimensional changes such as inner layer shrinkage or out-of-plane warpage of the PCB after cool-down [4]. These types of dimensional changes cause problems with chip insertion, solder connection, interconnection between layers and significantly reduce package reliability. In order to design more dimensionally stable boards, a better understanding of the substrate viscoelastic response is essential. Wang et al. [5] generated master relaxation curves for a 109 style composite substrate and reported different relaxation responses in the warp and fill directions. Shrotriya and Sottos [6] measured the creep compliance of 7628 style substrate in the warp and fill directions,

* Corresponding author.
E-mail address: shrotriy@iastate.edu (P. Shrotriya).

0266-3538/$ - see front matter © 2004 Elsevier Ltd. All rights reserved.
doi:10.1016/j.compscitech.2004.09.002

and correlated the difference in viscoelastic response to the weave architecture. Given the large number of different fabric styles used in the circuit board industry and the strong influence of weave architecture, further investigation is required to characterize the substrate creep and relaxation behavior with respect to different fabric styles. Since experimental viscoelastic characterization is not viable for every fabric style, micromechanical models are essential to predict the substrate properties from fiber, matrix and fabric properties.

Several micromechanical models have been developed for prediction of aligned fiber composite viscoelastic response using fiber and matrix properties [7–22]. The approximations used in the models involve: identifying an idealized unit cell, imposing representative boundary conditions on the unit cell, and inferring composite properties from solution of the resulting boundary value problem. For viscoelastic micromechanical modeling, the boundary value problem reduces to a set of integral equations that may be solved either by utilizing the correspondence between the equations of elasticity and the Laplace transformed linear viscoelastic equations [22], or numerically by methods such as finite element analysis (FEA). In the approach based on elastic–viscoelastic correspondence [9,13–16,18,20], viscoelastic mixing rules are obtained in the Laplace domain by replacing the elastic components in a given elastic model by their Laplace transform counterparts. The time dependent properties of the composite are obtained by inverse Laplace transform. In the FEA based approach [8,9], the viscoelastic boundary value problem is solved directly and the effective properties of composite are determined from the solution.

A myriad of micromechanical models for prediction of the elastic properties of woven composites have been reported in the literature [1,23–35]. Tan et al. [25] and Kuhn and Charalambides [23,24] presented an exhaustive literature survey on elastic micromechanical models for woven composites. Early micromechanical models used classical lamination theory (CLT) to determine the properties of an idealized unit cell that represented the warp and fill geometry. Ishikawa and Chou [26,27,36,37] formulated two 1-D models for predicting the elastic properties of a woven ply. The first model, the mosaic model, represents the fabric as an assemblage of two-ply crossply laminates, neglecting the continuity and undulation of the fiber bundles. CLT is used to calculate the compliance or stiffness of the crossply laminate and the effective properties are obtained through integration along the length of the unit cell. The second model, the crimp model, uses CLT to determine the properties of a thin slice and integrates the properties along the length of the unit cell. Almost ten years later, Naik and Shembekar [29–31] and Shembekar and Naik [38,39] presented a new model based on the crimp model. The improved model allows for gaps between the fiber bundles, in-plane misalignments between the piles, and the 2-D nature of plain weave laminae.

Sottos et al. [1] introduced two simple models to predict the properties of woven laminates. The first model is based on an equivalent laminate concept that idealizes the woven fabric laminate as a symmetric three-ply crossply laminate. The properties of the outer plies are calculated by combining warp fiber and resin properties via self-consistent micromechanics. Average ply properties for the undulating warp fibers are obtained by integrating over the length of unit cell. The inner ply properties are calculated in a similar fashion by averaging the properties of the fibers in the fill direction. The overall properties of the laminate are then obtained using CLT. The second model does not use lamination theory to determine the final properties of the woven laminate. The fill fiber properties are combined with resin properties via self-consistent micromechanics. The average fill ply properties are determined by integration over the unit cell, as described above. Assuming the warp bundles reinforce this intermediate fill ply, Halpin–Tsai equations are used to combine the warp fiber properties and the calculated properties for the intermediate fill ply. Average composite properties are achieved by integrating the combined properties over the unit cell for the undulating warp fibers.

Lee and Harris [40] developed a mathematical model based on Euler–Bernoulli beam theory for prediction of the effective elastic properties of a composite with wavy layers. The wavy layer is modeled as a curved beam and the matrix is assumed to act as an elastic foundation. Under the application of a tensile force, the curved beam extends due to elastic deformation as well as the rigid body rotation associated with reduction of crimp. The elastic deformation is governed by the elastic properties of the beam while the matrix determines the rigid body motion. Deformation of the curved beam is calculated by minimizing the total potential energy of the curved beam and the elastic foundation. Effective modulus of the composite is determined on the basis of the calculated displacement field. Ito and Chou [41] modified the curved beam model to predict the effective properties of plain-weave laminates.

Fewer models have been reported for prediction of viscoelastic properties of woven composites. Govindrajan et al. [42] utilized the approach based on elastic–viscoelastic correspondence to extend an existing model [26] for prediction of the creep behavior of graphite/epoxy woven composites. They characterized the creep compliance of the composite, but were unable to measure the matrix response directly. Instead, the matrix response was determined by fitting predictions to the measured creep compliance. Recently, Zhu et al. [43] performed 3-D viscoelastic finite element simulations to predict viscoelastic properties of a woven composite.

In this paper, we explore several micromechanical approaches to predict the viscoelastic response of woven composite substrates used in PCBs. In the first part of this study, we take an analytical approach and apply the elastic–viscoelastic correspondence principle directly to previously reported elastic micromechanical models. In the second part, a finite element model is adopted to investigate the influence of boundary conditions and constituent properties on the woven composite viscoelastic response.

2. Composite substrate characterization

An accurate description of a woven composite substrate and its constituents' response is essential for the main objectives of this study: developing micromechanical models to predict woven composite properties. Extensive characterization of the composite substrate (7628 fabric style) was reported in a previous paper by the authors [6]. The fabric architecture and creep compliance of the composite in both the fill and warp directions as well as the creep compliance of neat epoxy (no glass) was measured. A brief summary of the substrate characterization is presented here.

The plain weave fabric is composed of two sets of interlaced orthogonal warp and fill fiber bundles. The warp and fill bundles have different sizes, crimp angles, and volume fractions, which are described by a^k, b^k, d^k and h^k (see Fig. 1) where k = w or f for the warp or fill direction, respectively. The aspect ratio $(a/b)^k$ and the crimp angle $(h/d)^k$ of the bundles were carefully measured and the results are listed in Table 1. Each value represents an average of ten different measurements. The aspect ratio and the crimp angle of the fill direction fiber bundles are larger than those of the warp direction bundles. No consistent variations in the bundle size or crimp were observed at different locations across the board. Individual volume fractions of the warp and fill yarns were calculated from the manufacturer's specifications and are listed in Table 1. Yarn volume fraction in the fill and warp bundles (packing fraction) calculated from the measured bundle aspect ratio and manufacturer's specification, are also listed in Table 1.

Shrotriya and Sottos [6] reported the creep compliance and stress relaxation modulus of the neat FR-4 epoxy (no glass) and 7628 style composite substrate in the warp and fill direction. Creep compliance of neat epoxy and composite was measured at several temperatures between 30 and 160 °C using a Dynamic Mechanical Analyzer (Perkin–Elmer DMA 7e). Neat epoxy specimens were tested in three-point bending and thin single lamina specimens of composite were tested in uniaxial tension. Creep compliance data for the different temperatures were shifted using the time–temperature superposition principle to form the master creep compliance curves shown in Fig. 2(a). Shift functions for all the three cases show similar behavior. Logarithm of the shift function is bi-linearly dependent on the reciprocal of temperature as shown in equation below

Table 1
Measurements of bundle size and crimp

Aspect ratio a/b		Crimp h/d		Volume fraction v_f		Packing fraction k_f	
Fill	Warp	Fill	Warp	Fill	Warp	Fill	Warp
7.26	5.26	0.083	0.053	0.194	0.268	0.759	0.754

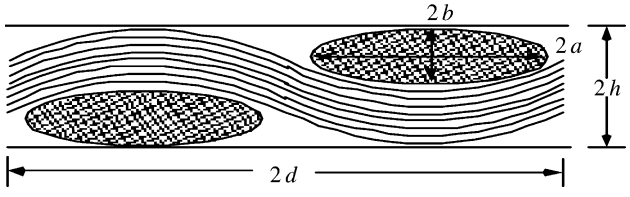

Fig. 1. Schematic of plain weave composite.

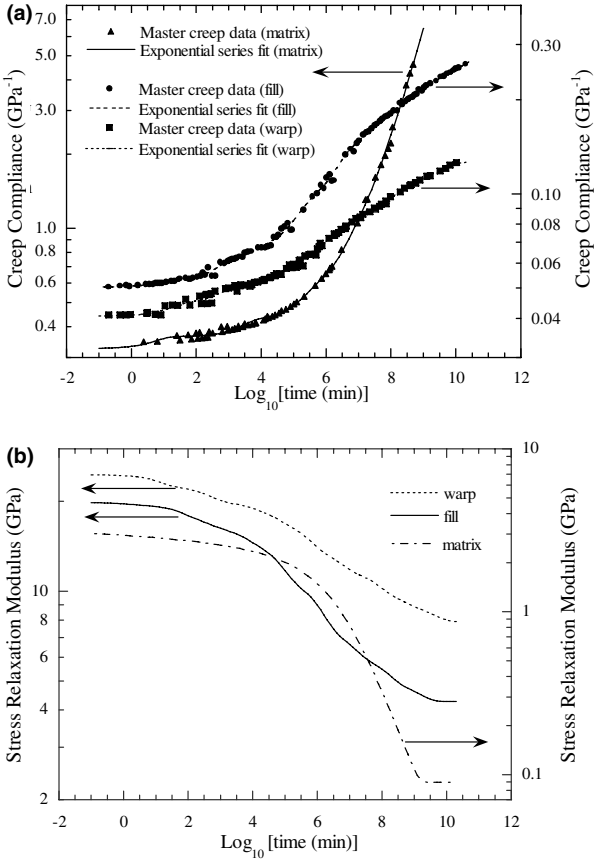

Fig. 2. Viscoelastic response of matrix and composite: (a) measured creep compliance of matrix and composite along the warp and the fill direction, (b) stress relaxation modulus of matrix and composite along the warp and the fill direction.

$$\mathrm{Log}(a_T(T)) = \begin{cases} -\frac{5757}{T} + 19, & T < 393\ \mathrm{K}, \\ -\frac{20661}{T} + 57, & T > 393\ \mathrm{K}. \end{cases} \quad (1)$$

Creep compliance data was converted to stress relaxation modulus in the Laplace domain. Stress relaxation modulus of the epoxy matrix and composite in the warp and fill directions plotted in Fig. 2(b), were obtained by inverse Laplace transform.

3. Analytical micromechanical models

3.1. Viscoelastic equivalent laminate

The first viscoelastic micromechanical model is based on the equivalent laminate model developed by Sottos et al. [1]. The model, shown schematically in Fig. 3, idealizes the woven fabric laminate as a symmetric three-ply crossply laminate. The fibers along warp and fill directions of the unit cell are separated and represented as three individual plies. The plies are arranged as a symmetric crossply laminate with the fill ply of thickness b^{f}, sandwiched between two warp plies of thickness $b^{\mathrm{w}}/2$ each. The effective stiffness matrix for each ply is calculated in the Laplace domain following the procedure described below.

Self-consistent relationships (see Appendix A) are used to calculate the transversely isotropic properties of a small segment dx. The fibers are assumed straight over the small segment and oriented at an angle θ to the xz coordinate system. The Laplace transformed stiffness components for the system are given by

$$C^{\mathrm{k}}_{ij}(s,x') = f(sE_{\mathrm{m}}(s), E_{\mathrm{f}}); \quad i,j = 1,2,6, \quad (2)$$

where k = w or f for warp or fill ply, $sE_{\mathrm{m}}(s)$ is the Laplace transformed matrix modulus and E_{f} is the fiber modulus. The weave geometry (Table 1) is used to describe the undulation of the fibers, and coordinate transformations are used to determine the rotated stiffness $C'^{\mathrm{k}}_{ij}(s,x)$ of the small segment, at a position x along the length of the ply. The effective stiffness matrix of the warp and fill plies is computed by assuming either iso-stress or iso-strain conditions along the length of the ply. In the case of iso-strain assumption, the individual ply stiffness matrix is computed by integrating the rotated stiffness along the length of the ply as follows:

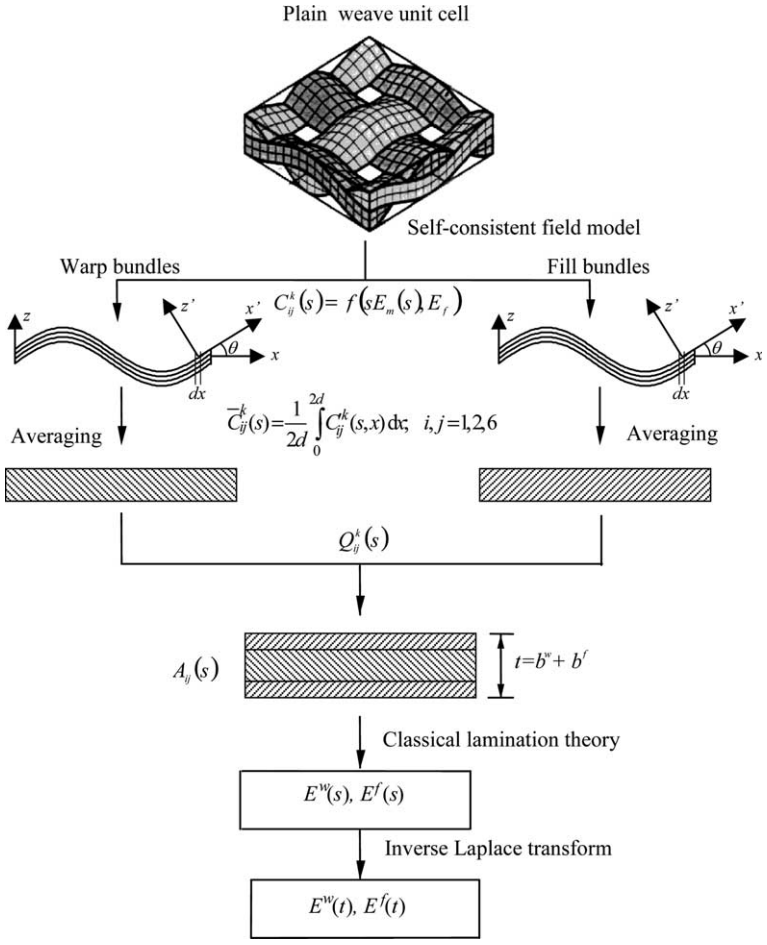

Fig. 3. Schematic of equivalent laminate model.

$$\overline{C}_{ij}^{k}(s) = \frac{1}{2d}\int_0^{2d} C_{ij}'^{k}(s,x)\mathrm{d}x; \quad i,j = 1,2,6, \tag{3}$$

where the length d is shown in Fig. 1. For the iso-stress assumption, the ply compliance matrix is computed by integrating the rotated compliance along the length of the ply and subsequently, inverted to obtain the stiffness matrix.

The laminate stiffness matrix, A_{ij}, is calculated from the stiffness matrices of the plies using CLT. The Laplace transformed stress relaxation moduli, $E^{f}(s)$ and $E^{w}(s)$, are determined from the laminate stiffness matrix and inverse Laplace transforms yield the stress relaxation moduli of the woven composite. The elastic properties of the glass fibers and FR-4 epoxy matrix listed in Table 2, and the bundle crimp, size and volume fraction listed in Table 1 were used to calculate the unrelaxed moduli. The values predicted by both iso-stress and iso-strain assumptions are compared with measured values in Table 3. The model predictions assuming iso-stress conditions are lower than the experimental values for both the fill and warp directions and the predictions corresponding to iso-strain conditions are consistently higher than experimental measurements.

The matrix relaxation modulus and the geometric properties of the weave from Table 1 were substituted into the viscoelastic equivalent laminate model in order to compute creep compliance of the composite along warp and fill directions. Predicted responses corresponding to both iso-strain and iso-stress assumptions in the viscoelastic equivalent laminate model are compared with experimental data in Figs. 4 and 5 for the fill and warp directions, respectively. Because of differences in the prediction of the unrelaxed response discussed above, the curves in Figs. 4 and 5 are normalized by the corresponding value of the unrelaxed response (Table 3) in order to facilitate the comparison of time-dependent response. The predictions corresponding to the iso-strain assumption underestimate the viscoelastic relaxation of the composite. As shown in Figs. 4 and 5, the predicted increase in creep compliance is significantly lower than the experimental measurements for both the fill and warp directions. Similarly, the model predictions corresponding to iso-stress assumption overestimate the viscoelastic relaxation and the calculated creep compliance increases much more rapidly than the measured response at long times. Neither the model predictions assuming iso-stress or iso-strain conditions effectively capture the viscoelastic response of the woven composite.

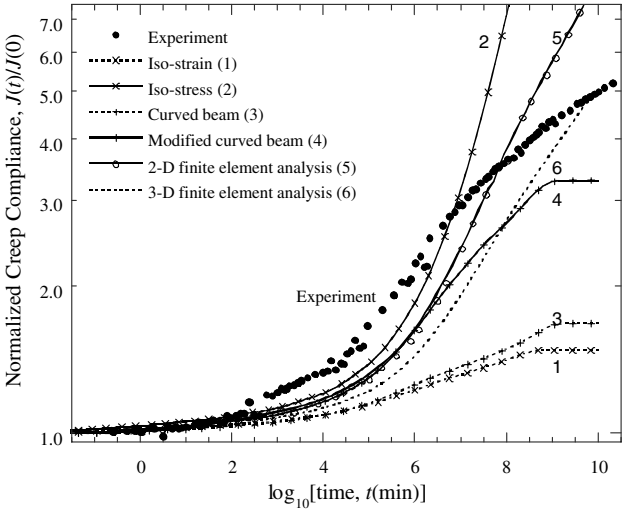

Fig. 4. Comparison of the experimental and predicted creep compliance along the fill direction for the micromechanical models.

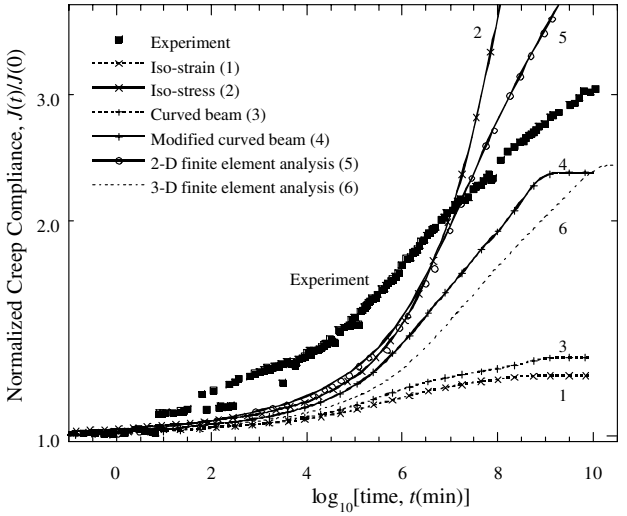

Fig. 5. Comparison of the experimental and predicted creep compliance along the warp direction for the micromechanical models.

Table 2
Elastic properties of glass fibers and epoxy matrix

Property	Glass fiber	FR-4 epoxy
E (GPa)	72.3	3.05
v	0.22	0.33

Table 3
Unrelaxed modulus of 7628 composite

Method	E_k (GPa)	
	Warp	Fill
Experiment	24.5 ± 0.5	19.8 ± 0.5
Viscoelastic equivalent laminate (iso-strain)	25.1	20.9
Viscoelastic equivalent laminate (iso-stress)	23.4	18.2
Curved beam on viscoelastic foundation	23.4	19.2
Modified curved beam on viscoelastic foundation	21.7	16.4
2-D finite element method (traction free)	21.5	16.8
2-D finite element method (symmetric)	27.2	21.7
3-D finite element method (traction free) [43]	23.4	19.7

3.2. Curved beam on a viscoelastic foundation

The inherent assumptions of viscoelastic equivalent laminate model preclude influence of extension-flexure coupling due to the undulating bundles on the woven composite deformation. A second analytical model was considered to better understand the role of the extension-flexure coupling on creep compliance predictions. This model, shown schematically in Fig. 6(a), is based on the curved beam model developed by Lee and Harris [40]. The fabric unit cell is divided into thin slices along the transverse direction. For a slice of thickness dy at the position y, the plain weave is separated into longitudinal and transverse fiber bundles. The longitudinal bundle is modeled as a wavy layer. The transverse fiber bundle and matrix are homogenized to form an effective matrix. The bundle geometry and volume fractions (listed in Table 1) were used to determine the volume fraction of glass fibers in the longitudinal bundle and the effective matrix. The properties of the effective matrix and the longitudinal bundle were calculated using self-consistent micromechanical relationships (Appendix A).

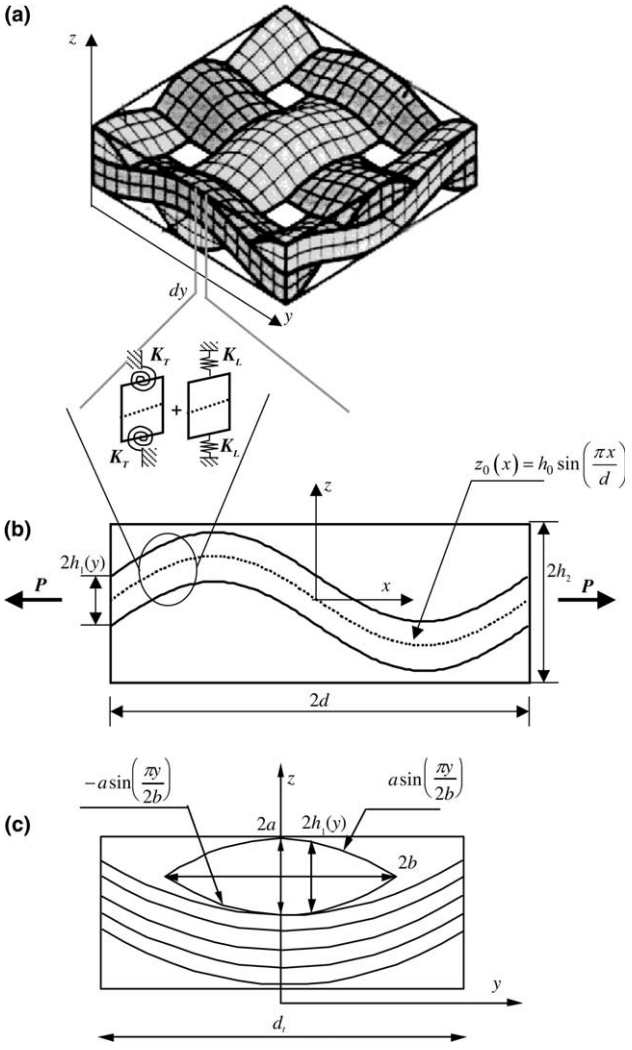

Fig. 6. Curved beam model: (a) schematic of the modulus calculation, (b) schematic of matrix load transfer, (c) Schematic of transverse crossection.

Following the elastic analysis presented by Lee and Harris [40], the deformation of the undulating wavy layer embedded in the effective matrix is determined by minimizing the total potential energy in the Laplace domain. The deflection $z_1(x, y)$ of the wavy layer from the centerline under the application of a tensile loading P (force per unit thickness) is governed by the following differential equation:

$$E_L I(y)\frac{d^4 z_1}{dx^4} - \left(\alpha^2(y)K_T(y) + P\right)\frac{d^2 z_1}{dx^2} + K_L(y)z_1 = P\frac{d^2 z_0}{dx^2}, \tag{4}$$

where

$$K_T(y) = 2(h_2 - h_1(y))G_m,$$
$$K_L(y) = \frac{2E_m}{(h_2 - h_1(y))},$$
$$\alpha(y) = \frac{2h_1(y)}{(h_2 - h_1(y))},$$
$$I(y) = \frac{2}{3}h_1(y)^3,$$

and $E_L I(y)$ is the flexural rigidity of the wavy layer. The torsional and linear spring constants of the effective matrix layer in the slice are $K_T(y)$ and $K_L(y)$, respectively. The shear and Young's moduli of the effective matrix are G_m and E_m, respectively. Deformation kinematics of the matrix layer was used to compute $\alpha(y)$, which is assumed constant for each slice. The geometric characteristics of the slice, h_0, $h_1(y)$, h_2, and d, are shown in Fig. 6(b).

The solution of Eq. (4) is given by

$$z_1(x, y) = \frac{h_0 \sin(\pi x/d)}{1 + \gamma(y)}, \tag{5}$$

where

$$\gamma(y) = \frac{\alpha(y)^2 K_T(y)}{P} + \left(\frac{\pi}{d}\right)^2 \frac{E_L I(y)}{P} + \left(\frac{d}{\pi}\right)^2 \frac{K_L(y)}{P}.$$

The extension due to change of crimp, the extension due to elastic deformation of the wavy layer, and the total extension of the slice calculated using Eq. (5) and assuming that $1/\gamma(y) \ll 1$ are, respectively:

$$\Delta_1(y) = \frac{\pi^2 h_0^2}{2d\gamma(y)}, \tag{6}$$

$$\Delta_2(y) = \frac{Pd}{2E_f h_1(y)}, \tag{7}$$

$$\Delta(y) = \frac{\pi^2 h_0^2}{2d\gamma(y)} + \frac{Pd}{2E_f h_1(y)}. \tag{8}$$

Therefore, the total strain in the matrix layer and the slice is $\Delta(y)/d$, and in the wavy layer is $\Delta_1(y)/d$. The total force per unit thickness on the slice is $P + 2E_m(\Delta(y)/d)(h_2 - h_1(y))$ and the apparent strain in the slice is $\Delta(y)/d$. The modulus per unit thickness, $E(y)$, of the slice is

$$E(y) = \frac{1}{\left(\left(\frac{\pi h_0}{d}\right)^2 \frac{1}{\mu} + \frac{h_2}{E_L h_1(y)}\right)} + E_m\left(\frac{h_2 - h_1(y)}{h_2}\right), \tag{9}$$

where

$$\mu = \left(\frac{h_1(y)^2}{(h_2 - h_1(y))h_2}\right)2G_m + \left(\frac{\pi h_2}{2d}\right)\frac{2}{3}E_L\left(\frac{h_1(y)}{h_2}\right)^3 + \left(\frac{2d}{\pi}\right)\frac{2E_m}{(h_2 - h_1(y))} \tag{10}$$

and y is the position of the slice along the transverse direction.

The cross section of the longitudinal bundle was modeled using sinusoidal functions as shown in Fig. 6(c), so that the longitudinal bundle height $h_1(y)$ is given by

$$h_1(y) = \begin{cases} 0 & y > b \text{ or } y < -b, \\ a\sin\left(\frac{\pi y}{2b}\right) & -b \leqslant y \leqslant b. \end{cases} \tag{11}$$

The Laplace transformed relaxation modulus per unit thickness of the slice, $sE(s,y)$, was calculated by replacing the effective matrix properties E_L, E_m and G_m by the corresponding Laplace transformed viscoelastic properties $sE_L(s)$, $sE_m(s)$ and $sG_m(s)$ in Eq. (9). The Laplace transformed relaxation modulus was obtained by integrating $sE(s,y)$ over the unit cell thickness d_t (see Fig. 6(c)). Inverse Laplace transform was performed to obtain the composite relaxation modulus.

The elastic properties of the glass fibers and FR-4 epoxy matrix listed in Table 2, and the bundle crimp, size and volume fraction listed in Table 1 were used to calculate the unrelaxed moduli. Unrelaxed modulus values predicted by the curved beam model are slightly lower than the measured values in Table 3. In the curved beam model, the varying cross section along the transverse direction is taken into account but interlacing of the warp and the fill fibers is neglected. Consequently, the model underestimates the elastic (unrelaxed) stiffness of the plain weave composite.

The matrix relaxation modulus and the geometric properties of the weave from Table 1 were substituted into the curved beam model in order to compute creep compliance of the composite along warp and fill directions. Normalized creep compliance predictions are compared with the previous laminate model as well as experimental data in Figs. 4 and 5 for the fill and warp directions, respectively. Although the curved beam model accounts for the deformation of the composite due to extension of the curved beam and the rigid body motion associated with flexural deformation of the bundles, the predictions are similar to those of the iso-stress case of the equivalent laminate model. A slightly larger increase in the creep compliance is predicted at longer times but not nearly as large as observed experimentally [6].

A simple modification was considered to improve the viscoelastic predictions of the curved beam model. As formulated originally, the effective matrix is assumed to exert both tensile and shear forces on the curved beam representing the fiber bundle (see Fig. 6(b)). Hence, the torsional and linear spring constants (K_T and K_L) of the effective matrix have a strong influence on the way applied load is transferred to the undulating fiber bundle and consequently, the flexural deformation of the unit cell. At low temperatures or over short time duration, the matrix is rigid and can apply both tensile and shear force on the fiber bundle as assumed by the model. At high temperatures or over long time duration, however, the matrix is dominated by viscoelastic mechanisms and may undergo considerable deformation, indicating a very small linear spring constant. This effect is explored in a modified version of the beam model by setting the linear spring constant to zero, $K_L = 0$, and assuming the matrix only exerts shear forces on the undulating bundle.

The creep compliances of the composite were predicted according to the modified matrix load transfer. The unrelaxed moduli calculated with the modified beam theory are considerably lower than the experimental values in Table 2. This discrepancy may be explained by the earlier hypothesis that for short time duration, the matrix exerts both tensile and shear loads on the fiber bundles, and consequently, neglecting the tensile load transfer under predicts the elastic (unrelaxed) moduli. The normalized creep compliances are compared with other model predictions and experimental data in Figs. 4 and 5, for the fill and the warp directions, respectively. The time dependence of the modified model predictions are in much better agreement with the experimental data. The shape of the modified compliance curve is nearly identical to that of the experiments in the transition region from about 10^2 to 10^8 min, but is shifted to the left by approximately two decades in time.

4. Finite element based micromechanical model

A 2-D finite element model of the unit cell was developed to compare with the analytical predictions, as well as investigate the influence of variables such as localized shifts in the relaxation spectrum, Poisson relaxation and traction-free boundary conditions that cannot be incorporated into the analytical models. The 3-D microstructure of the plain weave lamina is shown schematically in Fig. 1(a). In order to simplify the unit cell representation, with a view towards performing several parametric

studies, the plain weave unit cell is approximated using 2-D unit cells, for each fabric direction (warp or fill). The longitudinal fiber bundle in each unit cell is of constant thickness,

$$h^{k}_{avg} = \left(8a^{k}b^{k}\right)/\left(\pi h^{k}d^{k}\right), \tag{12}$$

which is derived by preserving the corresponding bundle (fiber) volume fraction of the composite. The geometry of the fiber bundles is characterized by a^{k}, b^{k}, h^{k} and d^{k} as specified in Fig. 1. The other geometric characteristics of the unit cell (undulations of the longitudinal bundles, profile of the transverse bundles, unit cell thickness) were kept the same as the composite.

The FEA code developed by Zhu et al. [48] was used for the plane-strain analysis of two adjacent unit cells. Two cells, rather than a single one, were chosen for accurate calculation of the creep compliance. A uniformly distributed load was applied to the edge of the adjacent cell (cell B, Fig. 7(a)) for a prescribed period of time and the displacement history was monitored for the original cell (cell A, Fig. 7(a)). Although the heterogeneity in the woven microstructure causes variations in the deformation at the loading surface, the deformation of the adjacent surface between the cells is quite uniform. The creep compliance for the lamina is inferred solely from the displacement history of the original cell.

The matrix was modeled as isotropic viscoelastic with creep compliance characterized by the Prony series representation of relaxation curve in Fig. 2(b) [6,49]. Initially the value of Poisson's ratio for the matrix was assumed constant and equal to 0.33, the unrelaxed (room-temperature) value for FR-4 epoxy. The viscoelastic properties of the transversely isotropic fiber bundles were calculated using the elastic–viscoelastic correspondence principle and the micromechanical relations based on self-consistent field method (Appendix A).

The model was discretized using three-noded triangular elements. A mesh refinement procedure was repeated for meshes in both the fill and the warp directions until satisfactory numerical convergence of the results was achieved. The final meshes used for analysis consisted of 1072 elements and 1972 nodes for the fill direction model, and 1244 elements and 2249 nodes for the warp direction model. Since the meshes are similar, only the warp direction mesh is shown in Fig. 7(c).

4.1. Boundary conditions

Creep compliance curves of the composite are obtained by testing a single lamina with traction-free conditions on the lateral surfaces. Whereas in the analytical models, the fabric unit cell is considered as a repeating unit in a multilayer laminate and the associated boundary conditions will impose more constraint on the deformation compared to experiment. In order to study the influence of lateral boundary conditions on composite response, two different boundary conditions were investigated on the top and bottom surface of the finite element model: a traction-free boundary condition (Fig. 7(a)), as imposed in the actual experiment, and a symmetry boundary condition with fixed flat surfaces in the y-direction (Fig. 7(b)). For both sets of boundary conditions, the matrix was modeled as elastic and uniform load was applied to compute the composite unrelaxed modulus and displacement fields. The unrelaxed modulus of the composite along the warp and fill direc-

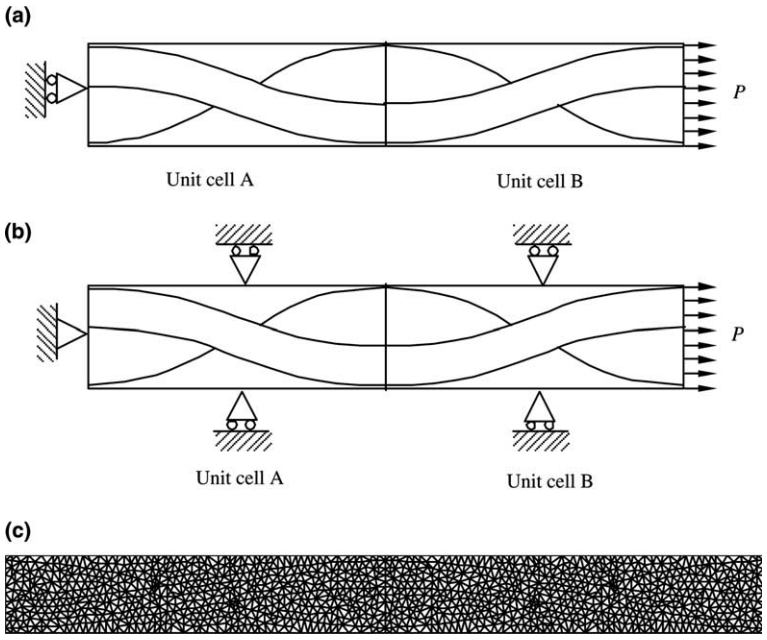

Fig. 7. Graphical representation of boundary conditions: (a) stress-free, (b) symmetric, (c) warp direction mesh of the two adjacent unit cells.

tions are presented in Table 3. The modulus predicted using the traction free boundary conditions are lower than the experimental measurements for both fill and warp directions. Part of this discrepancy may be due to the approximation of the plain weave lamina by a 2-D unit cell. The 2-D unit cell does not account for the interlaced bundle architecture and the varying cross section along the transverse direction [43]. Consequently, stiffness of the plain weave is underestimated. In contrast, the unrelaxed moduli corresponding to the symmetry boundary condition are higher than the experimental values. In the case of symmetry boundary condition, the maximum restraint is imposed on the unit cell and correspondingly, the modulus predictions are highest for both fill and warp directions.

The effect of these boundary conditions on the unrelaxed displacement field is shown in Figs. 8 and 9, for the fill and warp directions, respectively. Contours are plotted for both the u and v displacements. All of the calculated displacements are normalized by their respective maximum values and contours for fifteen intermediate values are plotted. As expected, the symmetry boundary conditions impose greater constraint on the deformation of the unit cell, particularly in the v fields (Fig. 8(a) and 9(a)).

The numerical displacement predictions are also compared to moiré interferometric measurements [49,50] in Figs. 8 and 9. A number of researchers have applied the moiré technique to investigate the local, heterogeneous deformation of textile composites [32,51,52]. Moiré interferometry is a full-field technique and each fringe corresponds to a constant line of displacement. The moiré images in Fig. 8 were acquired at 25 °C under a constant load of 20.1 MPa [49]. Comparison of the shape and distribution of both u and v field contours reveals that the traction-free boundary conditions most accurately predict the experimental fringe patterns. The displacement field generated under traction-free conditions is characteristic of deformation associated with bending loads (see for example Post et al. [51] and Stout [53]) and indicates that, even under uniaxial tensile load, the unit cell is subjected to localized flexural loading. Bending moments in the unit cell develop due to the undulations of fibers aligned in the loading direction. The anti-symmetric repeating pattern indicates that the neighboring unit cells are subjected to equal and opposite bending moments. The FEA model with traction-free boundary conditions accurately captures this deformation mechanism of the composite lamina. In contrast, the displacement fields calculated using symmetry boundary conditions are clearly not representative of the full-field measurements and indicate that any extension-flexure coupling of the unit cell deformation is suppressed for this case.

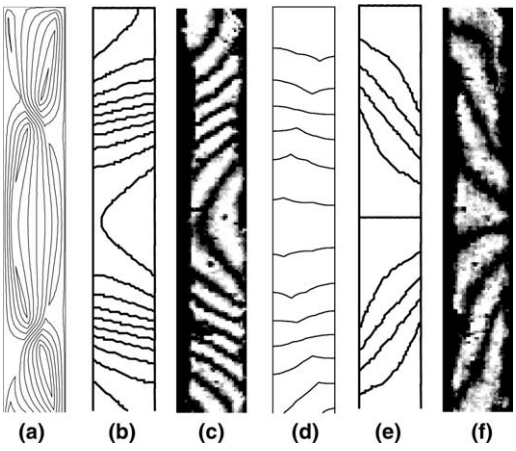

Fig. 8. Comparison of computed displacement field to moire images at 25° along Fill direction: (a) contour plot of v displacement corresponding to fixed boundary condition, (b) contour plot of v displacement corresponding to stress-free boundary condition, (c) moire image of v displacement, (d) contour plot of u displacement field corresponding to fixed boundary condition, (e) contour plot of u displacement field corresponding to stress free boundary condition, (f) moire image of u displacement field.

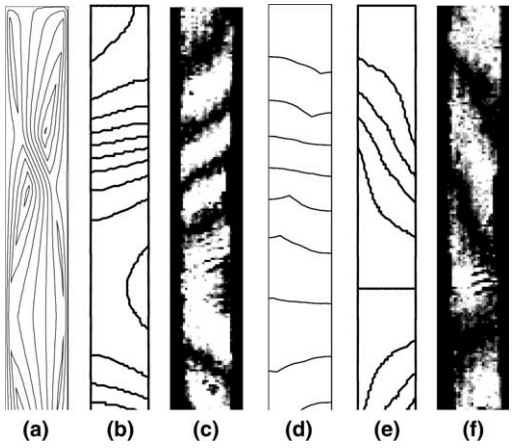

Fig. 9. Comparison of computed displacement field to moire images at 25° along warp direction: (a) contour plot of v displacement corresponding to fixed boundary condition, (b) contour plot of v displacement corresponding to stress-free boundary condition, (c) moire image of v displacement, (d) contour plot of u displacement field corresponding to fixed boundary condition, (e) contour plot of u displacement field corresponding to stress free boundary condition, (f) moire image of u displacement field.

4.2. Creep compliance

Successive simulations were run to create a master creep compliance curve for the lamina using time–temperature superposition. At each step in the simulation, the creep compliance of the lamina was calculated by applying a unit load over a short duration of time (10 min). Each step was performed at a particular temperature ranging from 25 to 160 °C (room temperature to above T_g), resulting in a sequence of creep compliance curves. All the compliance curves for different

temperatures were shifted to room temperature using the experimentally determined shift factors (Eq. (1)), thus forming a master compliance curve. As discussed earlier, the traction-free boundary conditions accurately captures the deformation mechanism of the lamina hence master curves were created only for this boundary condition.

Creep compliance predictions normalized with unrelaxed modulus are compared with the previous models as well as experimental data in Figs. 4 and 5 for the fill and warp directions, respectively. The predicted creep compliances are not in complete agreement with the experimental curves and the discrepancies are consistent for both fill and warp directions.

In the transition region adjacent to the unrelaxed regime (10^1–10^8 min), FEA predictions exhibit creep behavior similar to the iso-stress and modified curved beam model predictions. The numerical predictions increase by almost the same magnitude as experimental data but the time dependence (retardation spectrum) of the experimental data and predictions are clearly different. The numerical predictions more closely resemble the creep behavior of the matrix than the composite. In the transition region beyond 10^8 min, predicted compliances are significantly higher than the experimental data (see Figs. 4 and 5).

5. Parametric study

Creep compliance of the woven composite was predicted for four different parametric cases ranging from the limiting case of no relaxation (elastic) in the fiber bundles to relaxation predicted using the measured matrix response. The numerical predictions discussed previously and plotted in Figs. 4 and 5 are designated as case 5. For these calculations, bundle response was predicted using the measured matrix relaxation modulus and assuming a constant Poisson's ratio equal to 0.33. For a second case 5A, bundles were assumed to be elastic and bundle properties were predicted using the unrelaxed matrix modulus. Creep compliance of the composite was calculated using the elastic bundle properties and the measured matrix relaxation modulus. For a third case 5B, the influence of matrix Poisson relaxation on the composite viscoelastic properties was approximated assuming a constant matrix bulk modulus following O'Brien [57]. In cases 5 and 5B, the peaks of the relaxation spectrum for the bundle and the matrix were coincident. For the final case 5C, the bundle relaxation was modified from properties used for case 5B. Given the high volume fraction of fibers in the bundles (approximately 75 percent), there is an increased probability for surface effects to dominate the viscoelastic response. Motivated by the shifts reported by Sullivan et al. [47] and O'Brien [57], we modified the bundle response by shifting its peak relaxation spectrum to the left by two decades.

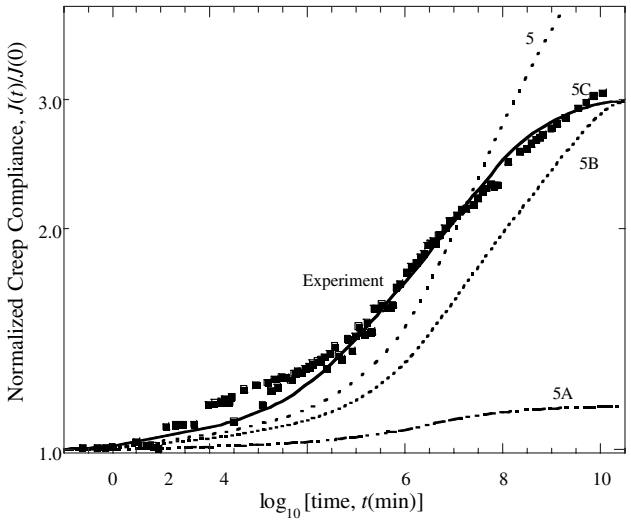

Fig. 10. Predicted creep compliance along warp direction for varying matrix response: (a) viscoelastic matrix with fixed Poisson's ratio, (b) elastic matrix in the fill and warp bundles, (c) viscoelastic matrix with constant bulk modulus and (d) viscoelastic matrix with constant bulk modulus and shifted retardation spectrum for matrix in fill and warp bundles.

Predicted compliance curves corresponding to all the cases are compared with the experimental data in Fig. 10 for the warp direction. As discussed previously for the viscoelastic bundle response (case 5), the predicted creep curves are shifted in time from the experimental data and the value of creep compliance at long time duration is almost an order of magnitude higher than the unrelaxed compliance. In great contrast, the creep compliance curves predicted assuming elastic bundle response (case 5A) exhibit almost no creep. Assuming constant bulk modulus for the matrix during viscoelastic relaxation (case 5B) significantly improves prediction of the fully relaxed compliance of the composite. The slope of the predicted creep curves in the transition region matches the experimental data, but the predicted curves are still shifted in time with respect to measured compliance. Modifying the relaxation spectrum of the bundle by a shift of two decades (case 5C), lead to significantly improved prediction of the experimental creep data.

6. Discussion

Among all the analytical models, the modified beam model is able to capture the general trend of viscoelastic creep behavior, but there are still discrepancies between theory and experiment. Experimental error may account for some of the difference between the experimental values and the model predictions. The inability to measure the creep response of the matrix at temperatures above

T_g may introduce experimental error in the matrix shift factors near T_g. Comparison of the matrix data with composite data measured at temperatures above T_g indicates that the experimental error in shift factors could be significant [6] but not sufficient to explain the large difference between the model predictions and experimental data. Moreover, the data in Figs. 4 and 5 indicate that the relaxation spectrum of the composite is shifted by two decades from that of the matrix. Such shifts have been reported previously in the literature [44–47] and may play a role in the current materials system. Another possible reason for the difference between analytical model predictions and experimental data is the assumption of constant Poisson's ratio for the matrix (Table 2).

Differences in the boundary conditions between the analytical model and experiments may also play a significant role. Experimental data are obtained by testing a single lamina with traction-free conditions on the lateral surfaces. In the micromechanical models, the fabric unit cell is considered as a repeating unit in a multilayer laminate and the associated boundary conditions will impose more constraint on the deformation compared to experiment. Because of difficulties in accurately modeling localized shifts in the relaxation spectrum, Poisson relaxation and traction-free boundary conditions in the analytical models, a 2-D finite element model of the unit cell was developed to study the influence of these variables on the predicted response.

The compliance curves predicted via FEA capture general experimental trends but there are still discrepancies between numerical predictions and little improvement over the analytical models. Part of this difference may be attributed to the use of a 2-D unit cell for both the FEA and the analytical models. However, recent 3-D FEA studies by Zhu et al. [43] of the same woven composite system reveal that 3-D analysis provides improved predictions of the unrelaxed and relaxed moduli (see Table 3 and Figs. 4 and 5) but the creep compliance is still not accurately captured. As shown in Fig. 4 for the fill direction, the 3-D FEA predicted creep curves are still shifted significantly from the measured values.

As mentioned previously (Section 3.2), localized shifts in the relaxation spectrum of the high volume fraction bundles or relaxation of Poisson's ratio may influence the accuracy of the predicted response. The surface of a reinforcement or filler has a measurable effect on the molecular and segmental mobility of a polymer matrix [54]. As a result, the mechanical properties and relaxation may be influenced by the presence of the reinforcement. Several researchers have observed differences in the relaxation or retardation spectra of a polymer matrix composite compared to that of the neat resin. Lipatov et al. [45,46] were among the first to report changes in the relaxation time spectra of filled polymer systems as a function of filler concentration. The average relaxation time of filled samples was shifted over two decades in time from unfilled samples. This shift was attributed to a selective sorption of one of the epoxy components on the filler surface before hardening. A surplus of the other component acted as plasticizer, causing a reduction of elastic modulus and a change in the relaxation behavior of the filled system. Similarly, Crowson and Arridge [44] observed a change in glass transition temperature between filled and unfilled epoxy systems. More recently, Palmese and McCullough [55] showed that a stoichiometric imbalance of epoxy resin and amine curing agent develops near fiber surfaces. For amine concentrations both above and below the stoichiometric point, the glass transition temperature of the polymer in that region was substantially reduced. Interferometric measurements reported by Sottos and Swindeman [56] for the same epoxy system indicated that a reduction in glass transition temperature near the fiber interface significantly influenced the time dependence of thermal deformations near the fiber surface. Sullivan et al. [47] measured the relaxation spectra of two different epoxies and their composites. They demonstrated that within the unrelaxed (glassy) and adjacent transition region, the spectra of the matrix and composites were similar to each other within a multiplicative constant. The presence of fibers altered only the magnitude component of the relaxation spectrum but not the relaxation time distribution component. However, at longer times, they showed that the peak of the composite relaxation spectra was shifted from that of the matrix because the presence of fibers suppressed the longer time relaxation mechanisms of the matrix. O'Brien [57] also found that the inclusion of unidirectional glass fibers in an epoxy matrix had a profound effect on the relaxation behavior. The temperature at which equilibrium could be reached during a ten minute creep test increased by more than 65 °C with an increase in fiber volume fraction from 0% to 63%. The shape of the composite creep compliance was shown to become less and less like the neat resin with increasing fiber content, and the retardation spectrum showed an increase in breadth as well as the emergence of a second peak.

Several authors have discussed the effect of time dependent Poisson's ratio on composite response [57–61]. Unfortunately, little data is available on time–temperature dependence of Poisson's ratio and small changes in Poisson's ratio are difficult to measure in the polymer matrix or composite. Tschoegl et al. [58] provide a critical review of Poisson's ratio in linear viscoelasticity and report on attempts to measure Poisson's ratio in polymers as a function of temperature. Lu et al. [62] investigated the uniaxial, shear, and Poisson relaxation of poly(methyl methacrylate) and successfully measured Poisson relaxation from an unrelaxed (glassy) value of 0.32 to a fully relaxed value of nearly 0.50. More recently, O'Brien [57] carried out a careful series

of interferometric experiments to measure time dependent Poisson's ratio in an aerospace structural epoxy and reported an increase from 0.4 (unrelaxed elastic response) to 0.48 (fully relaxed). Moreover, O'Brien showed that the influence of the time dependent matrix Poisson's ratio on prediction of composite creep compliance could be captured with surprising accuracy using the well known assumption of constant matrix bulk modulus [63].

Incorporation of an accurate bundle relaxation spectrum and matrix Poisson relaxation in the micromechanical models is limited by the lack of experimental data for the system of interest. There are no reported measurements of relaxation spectrum for the bundles (high volume fraction aligned fiber composite) or Poisson relaxation for FR-4 epoxy. Given the lack of data, a parametric study of these variables was performed using the FEA based micromechanical model, in order to ascertain the importance of the bundle relaxation spectrum and matrix Poisson relaxation in predicting viscoelastic properties.

Results of the parametric study demonstrate that the time dependence of the composite creep compliance is highly influenced by the time dependence of the local bundle properties as well as the matrix properties. Comparison of the predicted creep compliance curves with experimental data indicate that the viscoelastic response of the bundles may be different than that measured for the neat matrix due to the influence of the fiber surface on molecular mobility and relaxation processes in the polymer. Although the current study does not provide conclusive evidence of these changes in local properties, it does demonstrate that more careful characterization of bundle viscoelastic properties is needed for accurate modeling of woven composite viscoelastic response.

7. Conclusions

Micromechanical models were used for prediction of the viscoelastic response of woven composite substrates. Two different modeling approaches, based on the elastic–viscoelastic correspondence and on FEA, were utilized to predict the composite response. Previously reported elastic micromechanical models were modified using elastic–viscoelastic correspondence in order to predict the composite creep compliance. The models predicted an unrelaxed compliance close to the experimental results but did not accurately capture the relaxation of the composite. Comparisons of the model predictions with the experimental data clearly indicate that the creep compliance of the composite is dependent not only on the relaxation of the matrix, but also on boundary conditions of the unit cell.

FEA was also utilized to predict the creep compliance of the composite. The compliance was predicted for two different boundary conditions: traction-free in order to model the experiments and symmetric with fixed flat surfaces as a limiting case. Predictions corresponding to traction-free boundary conditions approximated the general trends of experimental curves but did not accurately match measured compliance response. Differences were due to the use of 2-D unit cells to approximate the plain weave lamina, micromechanical relations for approximating the bundle relaxation spectrum and the assumption that matrix Poisson's ratio is constant during relaxation. A parametric study was conducted in order to ascertain the influence of bundle response and matrix Poisson relaxation on the predicted creep compliance. The results indicate that the bundle relaxation spectrum and Poisson's ratio relaxation in the matrix need to be incorporated in order to predict the viscoelastic response of woven composites.

Acknowledgements

Financial support for the research was provided by Motorola Advanced Technology Center (Motorola Laboratories, Schaumburg) and the National Science Foundation. The authors also gratefully acknowledge Qi Zhu and Philippe H. Geubelle for helpful discussions about the finite element analysis.

Appendix A. Micromechanical relations based on self consistent field

The generalized self-consistent field equations for longitudinal modulus, major Poisson's ratio, in-plane shear modulus, bulk modulus, and transverse modulus are taken from Whitney and McCullough [22]. The relation for the transverse shear modulus was taken from Christensen [64].

1. Longitudinal Young's modulus (E_{11})

$$E_1 = E_{\mathrm{Lf}} v_{\mathrm{f}} + E_{\mathrm{m}} v_{\mathrm{m}}. \tag{A.1}$$

2. Poisson's ratio (ν_{12})

$$\nu_{12} = \nu_{\mathrm{LTf}} v_{\mathrm{f}} + \nu_{\mathrm{m}}(1 - v_{\mathrm{f}}). \tag{A.2}$$

3. In-plane shear modulus (G_{12})

$$G_{12} = G_{\mathrm{m}} \frac{[(G_{\mathrm{LTf}} + G_{\mathrm{m}}) + (G_{\mathrm{LTf}} - G_{\mathrm{m}})v_{\mathrm{f}}]}{[(G_{\mathrm{LTf}} + G_{\mathrm{m}}) - (G_{\mathrm{LTf}} - G_{\mathrm{m}})v_{\mathrm{f}}]}. \tag{A.3}$$

4. Transverse shear modulus (G_{23})

$$A\left(\frac{G_{23}}{G_{\mathrm{m}}}\right)^2 + 2B\left(\frac{G_{23}}{G_{\mathrm{m}}}\right) + C = 0, \tag{A.4}$$

where

$$A = 3v_f(1-v_f)^2\left(\frac{G_{23f}}{G_m}-1\right)\left(\frac{G_{23f}}{G_m}+\eta_f\right) + \left[\frac{G_{23f}}{G_m}\eta_m+\eta_f\eta_m-\left(\frac{G_{23f}}{G_m}\eta_m-\eta_f\right)v_f^3\right] * \left[=v_f\eta_m\left(\frac{G_{23f}}{G_m}-1\right)-\left(\frac{G_{23f}}{G_m}\eta_m+1\right)\right], \quad (A.5)$$

$$B = -3v_f(1-v_f)^2\left(\frac{G_{TTf}}{G_m}-1\right)\left(\frac{G_{TTf}}{G_m}+\eta_f\right) + \frac{1}{2}\left[\frac{G_{TTf}}{G_m}\eta_m-\left(\frac{G_{TTf}}{G_m}-1\right)v_f+1\right] \times \left[(\eta_m-1)\left(\frac{G_{TTf}}{G_m}+\eta_f\right)-2\left(\frac{G_{TTf}}{G_m}\eta_m-\eta_f\right)v_f^3\right] + \frac{v_f}{2}(\eta_m+1)\left(\frac{G_{TTf}}{G_m}-1\right) \times \left[\frac{G_{TTf}}{G_m}+\eta_f+\left(\frac{G_{TTf}}{G_m}\eta_m-\eta_f\right)v_f^3\right], \quad (A.6)$$

$$C = -3v_f(1-v_f)^2\left(\frac{G_{TTf}}{G_m}-1\right)\left(\frac{G_{TTf}}{G_m}+\eta_f\right) + \left[\frac{G_{TTf}}{G_m}\eta_m+\left(\frac{G_{TTf}}{G_m}-1\right)v_f+1\right] \times \left[\frac{G_{TTf}}{G_m}+\eta_f+\left(\frac{G_{TTf}}{G_m}\eta_m-\eta_f\right)v_f^3\right], \quad (A.7)$$

and

$$\eta_m = 3-4v_m, \quad \eta_f = 3-4v_{TTf}. \quad (A.8)$$

5. Plane strain bulk modulus (k_{23})

$$k_{23} = \frac{(k_{Tf}+G_m)k_m+(k_{Tf}-k_m)G_mv_f}{(k_{Tf}+G_m)-(k_{Tf}-k_m)v_f}. \quad (A.9)$$

6. Transverse Young's Modulus (E_2)

$$E_2 = \frac{1}{\frac{1}{4k}+\frac{1}{4G_{23}}+\frac{v_{12}^2}{E_1}}. \quad (A.10)$$

In the relations above E_p, G_p, k_p, v_p and v_p are Young's modulus, shear modulus, bulk modulus, Poisson's ratio and volume fraction, respectively and p = m or f for matrix or fiber.

References

[1] Sottos NR, Ockers JM, Swindeman M. Thermoelastic properties of plain weave composites for multilayer circuit board applications. J Electron Packaging 1999;121:37–43.

[2] Wu TY, Guo Y, Chen WT. Thermal–mechanical strain characterization for printed wiring boards. IBM J Res Develop 1993;37:621–34.

[3] Yuan J, Falanga LA. The in-plane thermal expansion of glass fabric reinforced epoxy laminates. J Reinforced Plastics Compos 1993;12:489–96.

[4] Shrotriya P, Sottos NR, Skipor AF. Residual stress development during relamination of woven composite circuit boards. J Compos Mater 2001;35:905–27.

[5] Wang TM, Daniel IM, Gotro JT. Thermoviscoelastic analysis of residual stresses and warpage in composite laminates. J Compos Mater 1992;26:883–99.

[6] Shrotriya P, Sottos NR. Creep and relaxation behavior of woven glass/epoxy substrates for multilayer circuit board applications. Polym Compos 1998;19:567–78.

[7] Agbossou A, Lagache M. Fiber distribution effects in linear viscoelastic behavior of polymer matrix composites: computation modelling and experimental comparison. Mech Res Commun 1998;25:105–15.

[8] Brinson LC, Knauss WG. Finite-element analysis of multiphase viscoelastic solids. J Appl Mech – Trans ASME 1992;59:730–7.

[9] Brinson LC, Lin WS. Comparison of micromechanics methods for effective properties of multiphase viscoelastic composites. Compos Struct 1998;41:353–67.

[10] Dzenis YA. Effective thermo-viscoelastic properties of fibrous composites with fractal interfaces and an interphase. Compos Sci Technol 1997;57:1057–63.

[11] Fisher FT, Brinson LC. Viscoelastic interphases in polymer-matrix composites: theoretical models and finite-element analysis. Compos Sci Technol 2001;61:731–48.

[12] Gosz M, Moran B, Achenbach JD. Effect of a viscoelastic interface on the transverse behavior of fiber-reinforced composites. Int J Solids Struct 1991;27:1757–71.

[13] Hashin Z. Viscoelastic behavior of heterogenous media. J Appl Mech 1965;32:630–6.

[14] Hashin Z. Viscoelastic fiber reinforced materials. AIAA J 1966;4:1411–7.

[15] Hashin Z. Complex moduli of viscoelastic composites: II. Fiber reinforced materials. Int J Solids Struct 1970;6:797–807.

[16] Jarzebski GJ. Viscoelastic properties of composite materials (celion, creep, fiberite, epoxy, resin, polyester). In: Chemical Engineering. University of Delaware; 1982.

[17] Schapery RA. On the characterization of nonlinear viscoelastic materials. Polym Eng Sci 1969;9:295–310.

[18] Schapery RA. Stress analysis of composite materials. J Compos Mater 1967;1:228–67.

[19] Li J, Weng GJ. Effect of a viscoelastic interphase on the creep and stress/strain behavior of fiber-reinforced polymer matrix composites. Compos Part B: Eng 1996;27B:589–98.

[20] Li J, Weng GJ. Effective creep behavior and complex moduli of fiber- and ribbon-reinforced polymer-matrix composites. Compos Sci Technol 1994;52:615–29.

[21] Lacabanne C, Levergne C, Michel L, Dufresne A, Martinez JJ, Boye J, et al. "Viscoelastic properties of composites". In: Presented at Composite Materials. Symposium A4 of the International Conference on Advanced Materials – ICAM 91, Strasbourg, France, 1991.

[22] Whitney JM, McCullough RL. Micromechanical materials modeling, Delaware composites design encyclopedia, vol. 2. Lancaster (PA): Technomic Publishing Company; 1990.

[23] Kuhn JL, Charalambides PG. Elastic response of porous matrix plain weave fabric composites. I. Modeling. J Compos Mater 1998;32:1426–71.

[24] Kuhn JL, Charalambides PG. Elastic response of porous matrix plain weave fabric composites. II. Results. J Compos Mater 1998;32:1472–507.

[25] Tan P, Tong L, Steven GP. Modelling for predicting the mechanical properties of textile composites – a review. Compos Part A 1997;28A:903–22.

[26] Ishikawa T, Chou TW. Stiffness and strength behaviour of woven fabric composites. J Mater Sci 1982;17:3211–20.

[27] Ishikawa T, Chou TW. Elastic behavior of woven hybrid composites. J Compos Mater 1982;16:2–19.

[28] Jiang Y, Tabiei A, Simitses GJ. Novel micromechanics-based approach to the derivation of constitutive equations for local/

global analysis of a plain-weave fabric composite. Compos Sci Technol 2000;60:1825–33.
[29] Naik NK, Shembekar PS. Elastic behavior of woven fabric composites. I. Lamina analysis. J Compos Mater 1992;26:2196–225.
[30] Naik NK, Shembekar PS. Elastic behavior of woven fabric composites. III. Laminate design. J Compos Mater 1992;26:2522–41.
[31] Naik NK, Shembekar PS. Elastic analysis of woven fabric laminates. II. Mixed fabric laminates. J Compos Technol Res 1993;15:34–7.
[32] Naik NK. Woven fabric composites. Lancaster (PA): Technomic Publishing Company; 1994.
[33] Whitcomb JD, Chapman CD, Srirengan K. Analysis of plain-weave composites subjected to flexure. Mech Compos Mater Struct 1998;5:41–53.
[34] Whitcomb J, Noh J, Chapman C. Evaluation of various approximate analyses for plain weave composites. J Compos Mater 1999;33:1958–80.
[35] Whitcomb JD, Chapman CD, Tang X. Derivation of boundary conditions for micromechanics analyses of plain and satin weave composites. J Compos Mater 2000;34:724–47.
[36] Ishikawa T, Chou TW. One-dimensional micromechanical analysis of woven fabric composites. AIAA J 1983;21:1714–21.
[37] Ishikawa T, Chou TW. In-plane thermal expansion and thermal bending coefficients of fabric composites. J Compos Mater 1983;17:92–104.
[38] Shembekar PS, Naik NK. Elastic behavior of woven fabric composites. II. Laminate analysis. J Compos Mater 1992;26:2226–46.
[39] Shembekar PS, Naik NK. Elastic analysis of woven fabric laminates. I. Off-axis loading. J Compos Technol Res 1993;15:23–33.
[40] Lee JW, Harris CE. A micromechanics model for the effective Young's modulus of a piecewise-isotropic laminate with wavy patterns. J Compos Mater 1988;22:717–41.
[41] Ito M, Chou TW. Elastic moduli and stress field of plain-weave composites under tensile loading. Compos Sci Technol 1997;57:787–800.
[42] Govindarajan S, Langrana NA, Weng GJ. An experimental and theoretical study of creep of a graphite/epoxy woven composite. Polym Compos 1996;17:353–61.
[43] Zhu Q, Shrotriya P, Geubelle PH, Sottos NR. Viscoelastic response of a woven composite substrate for multilayer circuit board applications. Compos Sci Technol 2003.
[44] Crowson RJ, Arridge RGC. The elastic properties in bulk and in shear of a glass bead reinforced epoxy resin composite. J Mater Sci 1977;12:2154–64.
[45] Lipatov YS, Babich VF, Rosovizky VF. Effect of filler on the relaxation time spectra of filled polymers. J Appl Polym Sci 1976;20:1787–94.
[46] Lipatov YS, Babich VF. Viscoelastic properties of interphase layers and laws governing their effect on the mechanical properties of composite materials. Mekhnika Kompozitnykh Materialov 1987;23:17–24.
[47] Sullivan JL, Wen YF, Gibson RF. Universal aspects of composite viscoelastic behavior. Polym Compos 1995;16:3–9.
[48] Zhu Q, Geubelle PH, Tucker III CL. Dimensional accuracy of thermocet materials: simulation of process-induced residual stresses. J Compos Mater 2001;35:2171–205.
[49] Shrotriya P. Dimensional Stability of Multilayer Circuit Boards. In: Department of Theoretical and Applied Mechanics. Urbana: University of Illinois at Urbana-Champaign; 2000. p. 141.
[50] Shrotriya P, Sottos NR. Local time–temperature-dependent deformation of woven composite. Experimental Mechanics 2004;44:336–53.
[51] Post D, Han B, Ifju PG. High senstivity moire. New York: Springer-Verlag; 1994.
[52] MirZadeh F, Reifsnider KL. Micro-deformations in C3000/PMR15 woven composite. J Compos Mater 1992;26:185–205.
[53] Stout EA, Sottos NR, Skipor AF. Mechanical characterization of plastic ball grid array package flexure using moiré interferometry. IEEE Trans Advanced Packaging 2000;23:637–45.
[54] Lipatov YS. Physical chemistry of filled polymers. International polymer science and technology monograph, 2. Shewbury, England: Rubber and Plastics Research Association of Great Britain; 1979.
[55] Palmese GR, McCullough RL. Effect of epoxy-amine stoichiometry on cured resin material properties. J Appl Polym Sci 1992;46:1863–73.
[56] Sottos NR, Swindeman M. Transient thermal deformations of the interphase in polymer composites. J Adhesion 1995;53.
[57] O'Brien DJ. In: Department of Mechanical Engineering. Urbana, USA: University of Illinois at Urbana-Champaign; 2003.
[58] Tschoegl NW, Knauss WG, Emri I. Poisson's ratio in linear viscoelasticity – a critical review. Mech Time-Dependent Mater 2002;6:3–51.
[59] Hilton HH. Implications and constraints of time-independent Poisson ratios in linear isotropic and anisotropic viscoelasticity. J Elasticity 2001;63:221–51.
[60] Hilton HH, Sung Y. The significance of (an) isotropic viscoelastic Poisson ratio stress and time dependencies. Int J Solids Struct 1998;35:3081–95.
[61] Viet HN, Pastor J. A semi-analytical resolution of a generalized unidirectional self-consistent model: theoretical bases and experiment in viscoelasticity. J Compos Mater 1998;32:2084–119.
[62] Lu H, Zhang X, Knauss WG. Uniaxial, shear, and Poisson relaxation and their conversion to bulk relaxation: studies on poly(methyl methacrylate). Polym Compos 1997;18:211–22.
[63] Ferry JD. Viscoelastic properties of polymers. 3rd ed. New York: J. Wiley and Sons; 1980.
[64] Christensen RM. A critical evaluation for a class of micro-mechancis model. J Mech Phys Solids 1990;38:379–404.